Catalysis Today 145 (2009) 45–54

Contents lists available at ScienceDirect

Catalysis Today

journal homepage: www.elsevier.com/locate/cattod

Application of a simple kinetic model for the oxidative coupling of methane to the design of effective catalysts

Jafar Sadeghzadeh Ahari [a], Reza Ahmadi [a], Hitoshi Mikami [c], Koji Inazu [c], Saeed Zarrinpashne [a], Shinichi Suzuki [b], Ken-ichi Aika [c,d,*]

[a] Research Institute of Petroleum Industry, Tehran, Iran
[b] Japan Oil, Gas and Metals National Corporation, Japan
[c] Interdisciplinary Graduate School of Science and Engineering, Tokyo Institute of Technology, Japan
[d] The Open University of Japan, Shimouma 4-1-1, Setagaya-ku, Tokyo 154-0002, Japan

ARTICLE INFO

Article history:
Available online 26 September 2008

Keywords:
Methane
Oxidation
Coupling
Kinetics
Catalyst design

ABSTRACT

Former research on the kinetics and/or mechanisms of the oxidative coupling of methane (OCM) was reviewed and given the following classification: (A) spectroscopic studies of O^- species and the reaction with methane, (B) kinetic simulation of gas phase reactions, (C) kinetic simulation of both gas phase and surface reactions, (D) kinetics integrating many radical reactions of single or several reactions, (E) surface kinetics focusing on methane consumption, and (F) power rate law expression of C2 (ethane and ethene) and C1 (CO and CO_2) formation. Each kinetic model has its own purpose; however, a method proposed by Iwamatsu and Aika (I–A model), belonging to the (D) classification, was chosen as a convenient model to relate the kinetics with the chemical or morphological nature of OCM catalysts. The I–A model was used to analyze the reaction over Na- or Li-doped oxide catalysts, which have been reported as effective catalysts, and the role of the catalyst components is discussed. The effect of alkali metal sulfates on the kinetics was also studied. Finally the selectivity and productivity of C2 compounds under high pressure (200 kPa) over these catalysts were simulated using the kinetic parameters obtained. Na_2CO_3/CaO, $LiNO_3$/La_2O_3–MgO, and three transition-based catalysts ($MnO/Na_2WO_4/SiO_2$, LiOH/$NiTiO_3$, and Na_2CO_3/$NiTiO_3$) were found to be effective under these industrial conditions.

1. Introduction

Since the rise in oil prices, attention has again been given to the utilization of natural gas through processes such as GTL (gas to liquid) or OCM (oxidative coupling of methane). The OCM reaction ($2CH_4 + 0.5O_2 = C_2H_6 + H_2O$, $2CH_4 + O_2 = C_2H_4 + 2H_2O$) was extensively studied, especially during 1980s; however, the one pass yield of total C2 compounds (C_2H_6 and C_2H_4) was lower than the economic threshold at that time. This situation might be changed in the near future, if the OCM reaction is reevaluated. If so, more practical data under pressures above atmospheric pressure may be necessary. Most of the researches during 1980s and 1990s were conducted under pressures below one atmosphere. Therefore, theories for the design of new catalysts must be investigated further, addressing practically and industrially applicable reaction conditions. The role of active sites has been studied extensively; however, other factors such as the effect of morphology have not been studied well. Since this reaction contains heterogeneously initiated gas phase reactions, the actual mechanism is most likely to be complicated.

The aim of this article is to discuss a simple kinetic model that might assist in the design of catalysts (role of catalyst elements in the reaction mechanism) and be useful for estimating the C2 yield under practical conditions (higher pressures). This prompts the question: what kinds of theories or methods would be useful? In order to answer this, we will firstly review past research on the kinetics with regard to the above criteria, and determine a method to apply to the design of practical OCM catalysts. Former research on the kinetics and/or mechanisms for the OCM reaction has been classified into six categories (A–F) as follows:

(A) Spectroscopic studies of O^- species relating to the reaction with methane [1–6]: the Lunsford Laboratory succeeded in producing O^- species on oxide surface defects through the introduction of N_2O. O^- species on an oxide surface were

* Corresponding author at: The Open University of Japan, Shimouma 4-1-1, Setagaya-ku, Tokyo 154-0002, Japan. Tel.: +81 3 5486 7701; fax: +81 3 5486 7705.
E-mail address: kenaika@c01.itscom.net (K.-i. Aika).

0920-5861/$ – see front matter © 2008 Elsevier B.V. All rights reserved.
doi:10.1016/j.cattod.2008.07.036

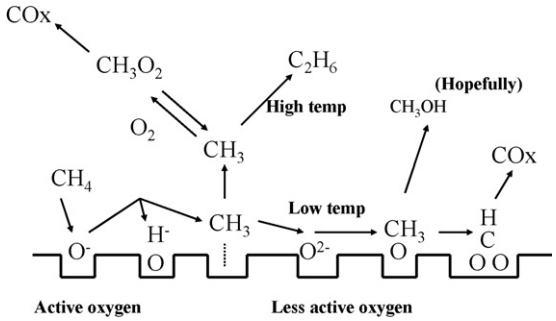

Fig. 1. Model for methane activation with two types of surface oxygen, active (such as oxygen anion radicals or adsorbed oxygen) and less active oxygen (such as lattice oxygen).

observed using electron paramagnetic resonance (EPR) spectroscopy and were reactive with methane even at room temperature. Aika and Lunsford found for the first time that the O^- species on MgO reacted with any alkane molecules in a one-to-one stoichiometry [1]. The O^- abstracts a hydrogen atom from methane to form methyl radicals, which finally decompose to CO and H_2 at room temperature [1], or combine together to form ethane at high temperature [2]. These studies provided the mechanistic base for the OCM reaction. Fig. 1 shows a schematic model for methane activation over an oxide surface; there are two types of oxygen, active and less active. A small number of active oxygen species such as O^- react with methane (a stable molecule). The methyl radical (unstable intermediate) formed has dual possibilities for reaction; recombination of methyl radicals (forming ethane) or reaction with (a large amount of) less active oxygen, such as lattice oxide or oxygen molecules. Thus, the nature of the lattice oxide controls the selectivity of the OCM reaction. The reactivity of lattice oxide with methyl radicals produced upstream was studied [4]. Since the lattice oxide of lanthanum oxide is less reactive, it allows methyl radicals to combine producing ethane, while methyl radicals are easily oxidized on the surface of ceria (reactive lattice oxide). The rate of destruction of methyl radicals is 10 times higher for ceria than that for lanthanum oxide [4]. Rate of reaction between methyl radical and surface oxygen has been studied under low pressure (0.4 Pa) condition [6].

(B) Kinetic simulation of gas phase reactions [7–10]: the OCM reaction occurs without catalysts at high temperature, although the selectivity for C2 is poor. The rate parameters of simple gas phase reactions have been established and seen in many books [7]. Theoretical simulations are possible using such parameters [8–10], and rather remarkable coincidence with the experimental results has been obtained. The selectivity for C2 molecules (ethane and ethene) is poor without a catalyst; however, these studies are useful to evaluate the contribution of gas phase reactions to the reaction with a catalyst, especially at high temperature and under high pressure. Calculation techniques are improved recently [11].

(C) Kinetic simulation of reactions including both gas phase and surface reactions [12–16]: gas phase reactions between methane and oxygen give (theoretically and experimentally) high CO/CO_2 ratios and high H_2 production compared to the reaction with a catalyst. In addition to the established gas phase (nearly 100) reactions, eight steps are proposed; three steps for the activation of methane at the catalyst surface supplying methyl radicals to the gas phase (oxygen activation, methyl radical formation, and water desorption), and five surface steps (methyl radical oxidation, ethane oxidation, formaldehyde oxidation, CO oxidation, and H_2 oxidation). The eight rate constants are successfully simulated to harmonize the total OCM reaction [14]. However, the selected rate data concerning the eight surface reactions cannot be easily evaluated, due to lack of the other data and complexity of the method. Therefore, these methods are not considered to be useful for practical catalyst design or process design. $TiSi_2$ (0.53 m^2/g) and $CoSi_2$ (2.01 m^2/g) catalysts show high C_2 yields (14.8 and 15%) at low temperature (823 K) and high pressure (0.35 MPa, 48% CH_4, 18% O_2, 34% H_2O). Pyatnitsky et al. have calculated the yields through similar calculation methods [16].

(D) Kinetics integrating many radical reactions to one or several reactions [17–24]: the feature of these studies is the use of a small number of elemental steps to explain the reaction performance in the low conversion region. Most of the research assumes that the reaction is composed of several steps, such as oxidation of methane (to produce methyl radicals or to complete oxidation), recombination of methyl radicals, and oxidation of methyl radicals. Some research assumes that the oxidation of methane occurs in the gas phase, on the surface, by parallel reactions, or by a series of reactions. The advantages of these kinetic models are the ease of analysis, so that data can be accumulated and compared with many other cases. Although the mechanism is applied only to the main steps, these models may be practical to compare the nature of various catalysts.

(E) Kinetics focusing on methane consumption [25–28]: research that has used simpler kinetic treatments than in the above category has been presented, where the rate of methane consumption is the main concern. Most of these studies were published at the earlier stage of OCM research. The analysis is simplistic; however, the relationship of C2 selectivity to the chemical nature of the catalyst is not the main concern.

(F) Power rate law expressions of C2 (ethane and ethene) and C1 (CO and CO_2) formation [29–32]: this is a typical style of reaction engineering, which is simplistic and can be easily applied to process design. This could be the most practical approach when the best catalyst is selected.

The research on the OCM reaction kinetics has been categorized into six types. Categories (D) and (F) appear to be simple and practical. The main difference between (D) and (F) is the presence of methyl radicals in the mechanism. For category (F), the intermediates are hindered, instead, the rate of any product formation can be expressed as a function of the reactant concentrations. The advantage of category (F) methods is that computer simulations can be applicable, even up to high conversion of methane. The disadvantage is that the rate constants have no physical meaning. Thus, it may not be practical for catalyst design. On the other hand, category (D) methods include the methyl radical concentration; therefore, the rate constants have physical meaning. In conclusion, category (D) is the most suitable for the design of OCM catalysts. This method can also predict the performance of catalysts, even at high pressure.

From the category (D) treatments, most of the mechanisms assume methyl radicals as intermediates and a steady state reaction [17,19,21–24], and some assume complete parallel reactions for C2 and C1 (CO and CO_2) production [20]. In this investigation, we are concerned with the former mechanism, because the methyl radicals can be oxidized depending on the reactivity of the oxide [4,6], as is illustrated in Fig. 1. The mechanism developed by Iwamatsu and Aika (I–A model) [17] will be used because of the simplicity. The contents of the model will be shown in the methods section. The disadvantage of this model is the lack of reaction analysis at high conversion, because the

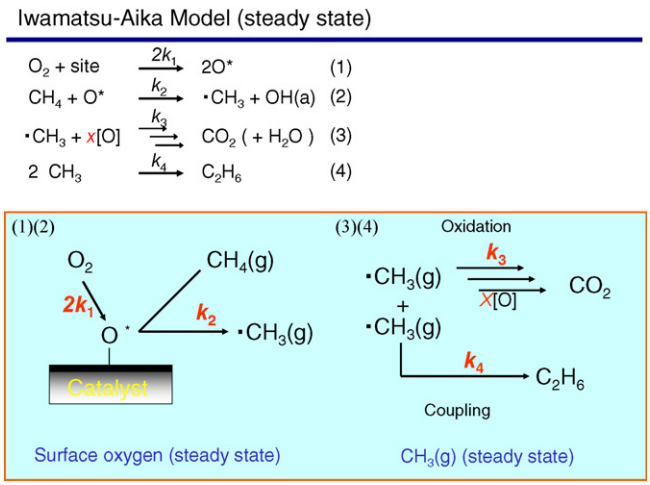

Fig. 2. The Iwamatsu–Aika model showing four steps and steady state condition.

reactions of C2 products are ignored. The kinetic analysis would become quite complicated if side reactions such as C2 oxidation were to be included. Wolf et al. [22–24] have proposed a sophisticated mechanism, where OH recombination step and C2 oxidation step are added to the mechanism used in the I–A model. The rate constants are simulated by solving non-linear equations assuming the steady state of elements. The calculation became possible using genetic algorism. The results are interesting and have proved OH concentration is negligible at the reaction temperature, which means that OH recombination does not affect the OCM reaction [22–24]. This method was not applied in the present work because of the complexity.

2. Methods

The I–A model [17] treats only four reactions, three of which are elementary steps (Eqs. (1), (2), and (4)) and the other is an empirical expression of the reaction between methyl radicals and x number of oxygen atoms (Eq. (3)). Fig. 2 illustrates the mechanism; oxygen molecules are activated on the surface (Eq. (1) with the rate constant of k_1), and methane reacts with the active oxygen to produce methyl radicals in the gas phase (Eq. (2) with the rate constant of k_2). The methyl radicals have two fates; recombination to produce C2 compounds (Eq. (4) with the rate constant of k_4), and oxidation to form CO_2 (and CO) (Eq. (3)). Realistically, for Eq. (3), numerous reactions (as is shown in category C) would be involved. However, for this examination, only one rate expression is assumed for the reactions between methyl radicals and x number of oxygen atoms (Eq. (3) with the rate constant of k_3).

The rate equation is expressed by the rate constant multiplied by the reactant concentration raised to the power of the stoichiometric number. The concentration of active surface oxygen O* is treated as unchanged under the steady state condition, as shown in Fig. 3. Through a steady state treatment (Eq. (5)), the concentration of active surface oxygen O* is obtained (Eq. (6)). The concentration of methyl radicals is also constant under the steady state condition (Eq. (7)), so that the concentration of methyl radicals can be determined (Eq. (8)).

The rates of C2 (Eq. (9)) and C1 formation (Eq. (10)) are obtained as shown in Fig. 4. The equations are so complex that abbreviated forms are used (Eq. (11)). The rate analysis is performed as follows: by comparing Eq. (9) with Eq. (10), new equations (Eqs. (12) and (13)) are obtained. Rate data were experimentally obtained by changing the O_2 or methane pressure. Using Eq. (12), the rate of C2 production is divided by the squared rate of C1 production, and can be plotted as a function of oxygen pressure on a log scale. Thus, $k_4/(k_3)^2$ and x are obtained independently (Eq. (12)). At the same time, the O_2 concentration divided by the methane consumption rate ($2R_2 + R_1$) can be plotted as a function of the O_2/CH_4 pressure ratio (Eq. (13)). The kinetic parameters k_1 and k_2 are obtained independently. An analysis method of this kind has already been successfully conducted by three research groups [17,19,21].

3. Experimental

3.1. Catalyst preparation

MgO, CaO, and La_2O_3 catalysts: suspensions of MgO (Ube Materials, ultra-fine 100A, 99.9%), CaO (Aldrich, 99.9%), or La_2O_3 (Aldrich, 99.9%) in distilled water were stirred at 353 K for 8 h until

Steady state treatment

For active surface oxygen

$$\frac{d\theta}{dt} = k_1 P_{O2}(1-\theta) - k_2 P_{CH4}\theta = 0 \quad (5)$$

$$\theta = \frac{k_1 P_{O2}}{k_1 P_{O2} + k_2 P_{CH4}} \quad (6)$$

For methyl radical in gas phase

$$\frac{dP_{\cdot CH3}}{dt} = \frac{k_1 P_{O2} k_2 P_{CH4}}{k_1 P_{O2} + k_2 P_{CH4}} - k_3 P_{\cdot CH3} P^{x/2}_{O2} - 2 k_4 P^2_{\cdot CH3} = 0 \quad (7)$$

$$P_{\cdot CH3} = \frac{k_3 P^{x/2}_{O2}}{4 k_4} \left(\left(1 + \frac{8 k_1 k_2 k_4 P_{O2} P_{CH4}}{k^2_3 P^x_{O2} (k_1 P_{O2} + k_2 P_{CH4})} \right)^{0.5} - 1 \right) \quad (8)$$

Fig. 3. Numerical derivation regarding steady state treatment.

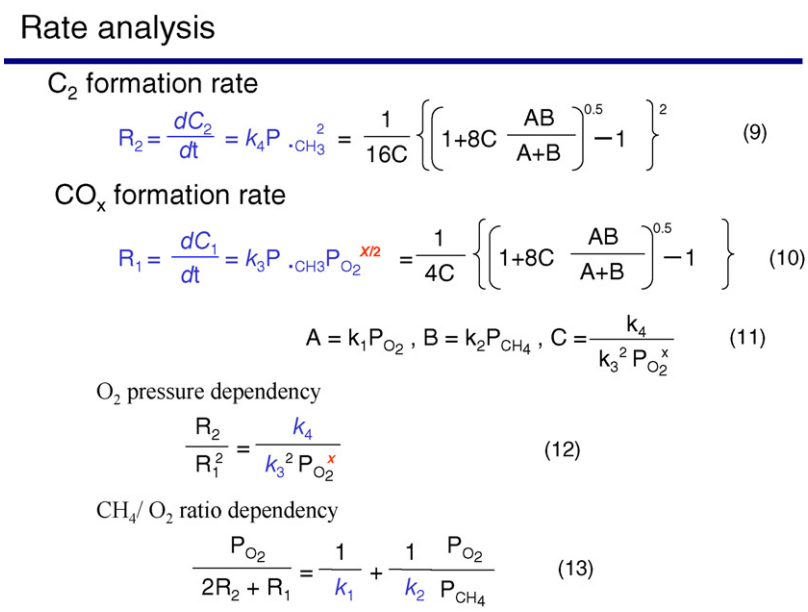

Fig. 4. Rate of C2 and C1 formation and the method of analysis.

a paste resulted. The MgO or La_2O_3 pastes were dried in air and heated at 673 K in a He atmosphere for 3 h. The CaO paste was dried overnight in air at 353 K and heated at 673 K in vacuo for 5 h. The surface areas of the prepared MgO and CaO were 157 and 42 m^2/g, respectively.

La_2O_3 and La_2O_3–MgO catalysts: an aqueous solution of $La(NO_3)_2{\cdot}6H_2O$ (Wako Pure Chem. Ind., 99.9%) was added to a 10% ammonia solution (Wako Pure Chem. Ind., special grade, 25%). The deposited hydroxide was dried overnight at 383 K, and then heated at 973 K for 5 h resulting in the formation of La_2O_3. A mixture of La_2O_3 and MgO was prepared to improve the catalytic activity. The same procedure for the preparation of La_2O_3 was used, with starting materials of $La(NO_3)_2{\cdot}6H_2O$ and $Mg(NO_3)_2$ (Wako Pure Chem. Ind., 99.9%). The La/Mg mole ratio was 25/75. The surface areas of the prepared La_2O_3 and La_2O_3–MgO were 10 and 13 m^2/g, respectively.

An aqueous solution of nitrate, hydroxide, sulfate, or carbonate of Li or Na was added to a heated water suspension of prepared MgO, CaO, La_2O_3, or La_2O_3–MgO powder, and stirred at 353 K until the water evaporated. The paste material was injection-molded from a syringe, dried, and then heated at 973 K in air. The procedure is similar to that previously reported [14,33,34]. The standard amount of alkali metal (Li and Na) added was 23 mol%, except for the addition of 5 mol% Li in $LiNO_3$/MgO (sample #1 in the tables). However, a significant amount of the alkali metal content is lost due to evaporation during the pretreatment process. It has been reported that approximately 40% of Na is lost after 3.5 h of heating in He at 1073 K [33].

$NiTiO_3$ catalyst: a suspension of $NiTiO_3$ (Aldrich, 99.9%) in distilled water was heated at 573 K with stirring. LiOH (Wako Pure Chem., 99.9%) or Na_2CO_3 (Wako Pure Chem., 99.7%) was added to the above $NiTiO_3$ solution, and heated at 573 K with stirring until a paste was formed. The paste was injection-molded from a syringe, dried, and then heated at 973 K in air. The procedure is similar to that reported in [19].

$Mn/Na_2WO_4/SiO_2$: Fang et al. [35] reported this type of catalyst as one of the most effective OCM catalysts. SiO_2 gel (Fuji Silica, 207 m^2/g) was added to an aqueous solution of $Mn(NO_3)_2{\cdot}6H_2O$ (Wako Pure Chem., 99.9%), stirred, and heated at 353 K, and then left at 353 K for 5 h to dry. An aqueous solution of $Na_2WO_4{\cdot}2H_2O$ (Wako Pure Chem., 99.9%) was added the prepared material, stirred and then heated overnight at 353 K to dry. The obtained material was heated at 1073 K for 8 h in air. The procedure is similar to that reported in [19].

3.2. Reaction rate measurements

Weighed catalysts (2.0 g standard) were placed between quartz wool in a tubular quartz reactor. The gas flow rate was controlled using mass flow controllers (Kofloc 3660). The heating furnace was controlled with a differential control system (Shimaden FP-21). The reaction products were analyzed using a micro gas chromatograph (GC; Agilent 3000A Micro GC). Nitrogen in air (Taiyo Toyo Sanso, Co.) was used as an internal standard. Catalysts were pretreated with a He (JHC, 99.9%) flow of 40 ml/min at 1073 K for 1 h. The standard reaction temperature was also 1073 K. Methane (Liquid Gas Ltd., 99.99%) and air (Taiyo Toyo Sanso, Co.) were used as reactants. The standard flow rates were 16/20/14 ml/min for CH_4/air/He ($CH_4/O_2 = 4$). Partial pressure dependency was studied by changing the flow rates of methane, air, and the balance gas, He.

3.3. Characterization

Brunauer–Emmett–Teller (BET) surface area was measured with a Belsorp 28SA (Japan Bell Ltd.) at 77 K using N_2. For those samples with small surface areas, Kr was used at 77 K. Samples were evacuated at 723 K for 1 h prior to measurement. X-ray diffraction (XRD) patterns were measured with a Rigaku Multiflex S diffractometer. Surface analyses of the pelletized catalysts were performed before and after the reaction using an X-ray photoelectron spectrometer (XPS; Ulvac-Phi 1700R). Cooled samples were transferred from the reactor to the XPS apparatus through a transfer chamber filled with nitrogen.

4. Results

4.1. General view of the initial catalyst activities

The catalysts examined are classified into two types; six non-redox oxide-based catalysts, $LiNO_3$/MgO, $NaNO_3$/MgO, Na_2CO_3/

Table 1
Oxidative coupling of methane over various catalysts at 1073 K

Catalyst (prepared form)	Conversion (%)		C_2 selectivity (%)	C_2 yield (%)	Carbon balance[a] (%)
	CH_4	O_2			
1 $LiNO_3/MgO$	19.1	80.5	55.5	10.6	100
2 $NaNO_3/MgO$	27.1	81.1	52.0	14.1	100
3 Na_2CO_3/CaO	25.0	94.8	43.6	10.9	83
4 Na_2SO_4/CaO	24.8	95.0	46.0	11.4	87
5 $LiNO_3/La_2O_3$	24.1	82.1	54.4	13.1	100
6 $LiNO_3/La_2O_3$–MgO	28.5	92.4	53.0	15.1	91
7 $MnO/Na_2WO_4/SiO_2$	21.9	71.6	58.0	12.7	100
8 $LiOH/NiTiO_3$	23.8	67.0	45.8	10.9	98
9 $Na_2CO_3/NiTiO_3$	15.3	60.3	47.6	7.3	91

Catalysts weight 0.2 g, CH_4/air/He = 16/20/14 ml/min, W/F = 0.82 g h/mol, measured after 30 min on stream.
[a] C_2 and CO_x yield divided CH_4 conversion.

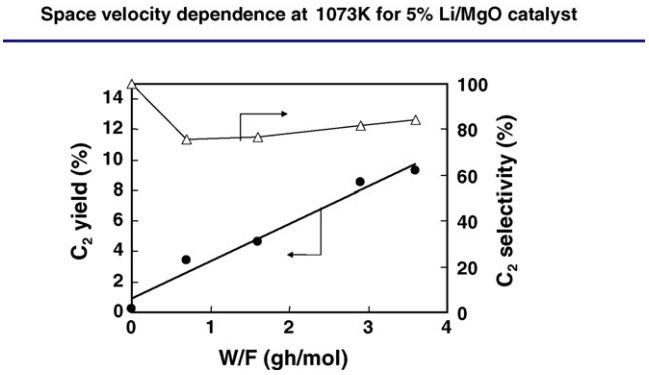

Fig. 5. C2 yield and C2 selectivity of the OCM reaction at 1073 K over 5% Li/MgO as a function of W/F (contact time).

CaO, Na_2SO_4/CaO, $LiNO_3/La_2O_3$, $LiNO_3/La_2O_3$–MgO, and three redox oxide-based catalysts, $MnO/Na_2WO_4/SiO_2$, $LiOH/NiTiO_3$, and $Na_2CO_3/NiTiO_3$. Since the activity decreases with time, especially for lithium-promoted catalysts, the data were measured from 30 min after the start of the reaction (90 min after raising the temperature to 1073 K). The reaction data of these catalysts under standard conditions are shown in Table 1. A synergistic effect was observed by the combination of a selective catalyst ($LiNO_3/MgO$) and an active catalyst ($LiNO_3/La_2O_3$), as reported for many mixed catalysts [36–41]. The C2 yield of $LiNO_3/La_2O_3$–MgO (15%) was higher than that before mixing (13% for $LiNO_3/MgO$ and 14% for $LiNO_3/La_2O_3$) (Table 1). The crystal size of La_2O_3 measured from the XRD-line broadening was found to become smaller, from 25 to 20 nm when mixed with MgO. These catalysts are mostly known as effective catalysts. Regardless, the purpose of this study is the application of kinetics, so that we shall not make further comments regarding the C2 yield or C2 selectivity under the standard conditions shown here.

4.2. Kinetic analysis of initial rate

Firstly, the OCM reaction over $LiNO_3/MgO$ was analyzed by changing the space velocity (F/W). In Fig. 5 the C2 yield (total yield of ethane and ethene) is plotted as a function of W/F (contact time). The C2 yield was shown to have a linear relationship with the contact time, up to W/F = 3.6 gh/mol. In this region, the contribution of secondary reactions such as C2 oxidation seems to be low, so that the I–A model is applicable.

The partial pressure dependency was studied over $LiNO_3/MgO$ by changing either the CH_4 pressure or O_2 pressure at a W/F of 3.6 gh/mol. The results are rearranged using Eqs. (12) and (13), and are shown in Fig. 6. The linearity of the two lines for each analysis was sufficient to exceed a least squares regression factor (R^2) of 0.95, indicating that the I–A model was applicable. Kinetic parameters, x, $\log(k_4/k_3^2)$, k_1, and k_2 were obtained, and are shown in Table 2.

In addition to $LiNO_3/MgO$, five non-redox oxide-based catalysts, $NaNO_3/MgO$, Na_2CO_3/CaO, Na_2SO_4/CaO, $LiNO_3/La_2O_3$, $LiNO_3/La_2O_3$–MgO, and three redox oxide-based catalysts, $MnO/Na_2WO_4/SiO_2$, $LiNO_3/NiTiO_3$, and $NaNO_3/NiTiO_3$ were kinetically studied using the I–A model. The results were rearranged using Eqs. (12) and (13), as in the case of $LiNO_3/MgO$. The linearity of the two lines for each analysis was sufficient to exceed a least squares regression factor (R^2) of 0.95, indicating that the I–A model was applicable. Kinetic parameters, x, $\log(k_4/k_3^2)$, k_1, and k_2 were obtained, and are shown in Table 2.

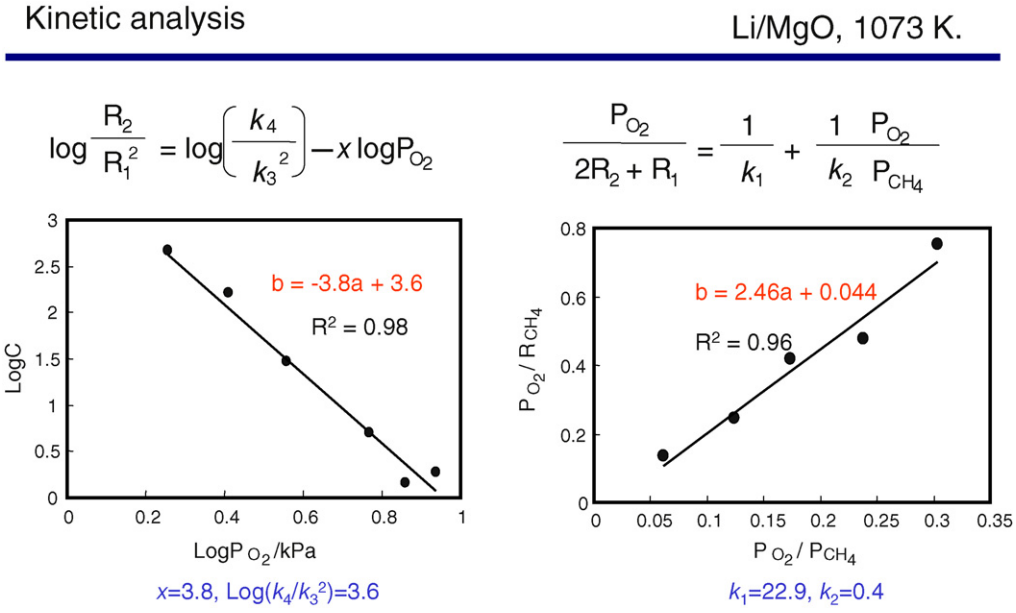

Fig. 6. Reaction rate analysis for 5% Li/MgO at 1073 K using the I–A model.

Table 2
Results of kinetic analysis for various catalysts

Catalysts (prepared form)	x	$\log(k_4/k_3^2)$	k_1	k_2
1 $LiNO_3/MgO$	3.8	3.6	22.9	0.4
2 $NaNO_3/MgO$	1.9	0.3	20.7	4.0
3 Na_2CO_3/CaO	1.5	0.3	34.8	7.0
4 Na_2SO_4/CaO	2.4	0.6	26.0	8.8
5 $LiNO_3/La_2O_3$	2.4	0.9	20.2	5.4
6 $LiNO_3/La_2O_3$–MgO	2.3	2.2	32.4	9.5
7 $MnO/Na_2WO_4/SiO_2$	1.5	0.8	5.2	2.9
8 $LiOH/NiTiO_3$	1.3	0.2	9.2	2.2
9 $Na_2CO_3/NiTiO_3$	1.7	1.2	20.7	2.0

k_1 and k_2 (mmol/kPa g h); k_4/k_3^2 (kPa^x g h/mmol). Reaction temperature was 1073 K and GHSV was 30,000 ml/g h.

The surface areas of the catalysts after the pretreatment were as follows: 2.9 m^2/g ($LiNO_3/MgO$), 4.5 m^2/g ($NaNO_3/MgO$), 2.3 m^2/g (Na_2CO_3/CaO), 3.3 m^2/g (Na_2SO_4/CaO), 1.4 m^2/g ($LiNO_3/La_2O_3$), 12.2 m^2/g ($LiNO_3/La_2O_3$–MgO), 2.2 m^2/g ($MnO/Na_2WO_4/SiO_2$), below 1 m^2/g ($LiNO_3/NiTiO_3$), and below 1 m^2/g ($NaNO_3/NiTiO_3$). The addition of alkali metals significantly reduces the surface area of the catalyst, as previously reported in [33].

4.3. Effect of lithium sulfate and reaction time

Li is known to be easily evaporated, which may result in the deactivation of a Li-promoted catalyst. Sulfate (a stable material), was used instead of nitrate for catalysts #1, #5, and #6 as has been reported elsewhere [42]. Table 3 shows the reaction performance for six catalysts after 2 h of reaction. Comparing the results (Table 3) for catalysts #1, #5, and #6, with those after 30 min (Table 1), the C2 yield for $LiNO_3/MgO$ is drastically decreased, and $LiNO_3/La_2O_3$ does have some C2 yield; however, the activity of $LiNO_3/La_2O_3$–MgO remained unchanged. After a 24-h run (not shown in Table 3), the C2 yields of the sulfate-promoted catalysts were observed to not decrease, at least for La_2O_3 (#11) and La_2O_3–MgO (#12). For some reason, the activity of Li_2SO_4/MgO (#10) was extremely low, and may be due to an excess amount of lithium covering the active sites of the catalyst. The lithium content is higher for #10 (23 mol%) than that for #1 (5 mol% when prepared). Lithium sulfate may be effective only for a La_2O_3-support. XRD analysis of these catalysts (added in Table 4) shows the formation of a new phase (lanthanum sulfate $(LaO)_2SO_4$), which suggests the following reaction: $Li_2SO_4 + La_2O_3 \rightarrow (LaO)_2SO_4 + Li_2O$. Although lanthanum sulfate, $(LaO)_2SO_4$, itself is not the reactive phase [42], it may help to stabilize the lithium oxide.

The amount and state of lithium during the reaction were studied using XPS and are shown in Fig. 7. Unexpectedly, the surface lithium content is not significantly changed during the reaction, except for $LiNO_3/La_2O_3$ (#5). The activity change does not seem to be related with lithium content. However, it should be noted that XPS measurements provide information only for several layers of the surface. Most of the lithium content may be oxide or hydroxide; however, those amorphous phases cannot be identified by XRD (Table 4). Some of the lithium exists as carbonate (Fig. 7) (and sulfate (XRD analysis shown in Table 4)) due to the reaction with product CO_2 (#10–12).

Table 3
Effect of sulfate promotion of lithium on the reaction performance for a 2-h run[a]

Catalyst[b]	Conversion (%)		C_2 selectivity (%)	C_2 yield (%)	Carbon balance (%)
	CH_4	O_2			
(1) $LiNO_3/MgO$[c]	7.9	24.5	58.5	4.6	94
(10) Li_2SO_4/MgO	2.1	4.5	72.4	1.5	96
(5) $LiNO_3/La_2O_3$	20.5	90.0	45.2	9.3	100
11 Li_2SO_4/La_2O_3	22.2	78.5	59.9	13.3	100
(6) $LiNO_3/La_2O_3$–MgO	24.2	85.7	58.8	14.9	99
(12) Li_2SO_4/La_2O_3–MgO	25.8	88.0	64.3	16.6	100

[a] Catalysts weight 0.2 g, CH_4/air/He = 16/20/14 ml/min, W/F =0 .82 g h/mol, measured after 2 h on stream at 1073 K.
[b] Li content: 23 mol%.
[c] As reference.

Table 4
Effect of sulfate promotion of lithium on the kinetic performance for a 2-h run[a]

Catalysts (states after pretreatment from XRD)	x	$\log(k_4/k_3^2)$	k_1	k_2
(1) $LiNO_3/MgO$ (MgO)	3.8	3.2	11.2	2.6
10 Li_2SO_4/MgO (MgO, Li_2SO_4)	–	–	–	–
(5) $LiNO_3/La_2O_3$ (La_2O_3)	1.7	0.5	15.1	2.2
11 Li_2SO_4/La_2O_3 (La_2O_3, Li_2SO_4, $(LaO)_2SO_4$)	2.7	1.4	9.1	2.9
(6) $LiNO_3/La_2O_3$–MgO (MgO, La_2O_3)	1.9	0.9	17.4	2.6
12 Li_2SO_4/La_2O_3–MgO (MgO, La_2O_3, Li_2SO_4, $(LaO)_2SO_4$)	2.7	1.2	11.7	5.5

k_1 and k_2 (mmol/kPa g h); k_4/k_3^2 (kPa^x g h/mmol).
[a] Reaction temperature was 1073 K and GHSV was 30,000 ml/g h.

4.4. Kinetic analyses of the reaction after a 2-h run

Kinetic analyses using the I–A model were also successful for the catalysts listed in Table 3. The kinetic parameters obtained are shown in Table 4. It should be noted that the kinetic parameters for the $LiNO_3$-promoted catalysts (#1, #5, and #6) after a 2-h run were different from those for the initial state (30 min). The effect of reaction time on the kinetic parameters was observed, and this will be discussed later.

5. Discussion

5.1. Relation between the kinetic parameters and chemical nature of the catalysts

The catalysts used for the kinetic analysis in this study have already been reported elsewhere as effective for the OCM reaction [36–41]. The C2 yield and selectivity (Table 1) under standard conditions were high as has been reported. The purpose of this study is not to evaluate these values, but to analyze the kinetic parameters shown in Table 2.

Firstly, k_2 is plotted as a function of k_1 in Fig. 8. As the model in Fig. 2 shows, catalysts with high k_1 and k_2 values can produce a large number of methyl radicals per unit of time. In this sense, the Na-promoted CaO (#3and #4) and Li-promoted La_2O_3–MgO (#6)

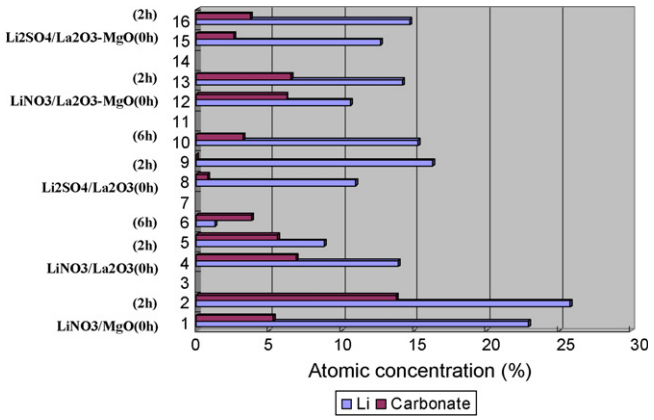

Fig. 7. Surface lithium and carbonate contents of five catalysts as a function of reaction time observed using XPS. (For interpretation of the references to color in this artwork, the reader is referred to the web version of the article.)

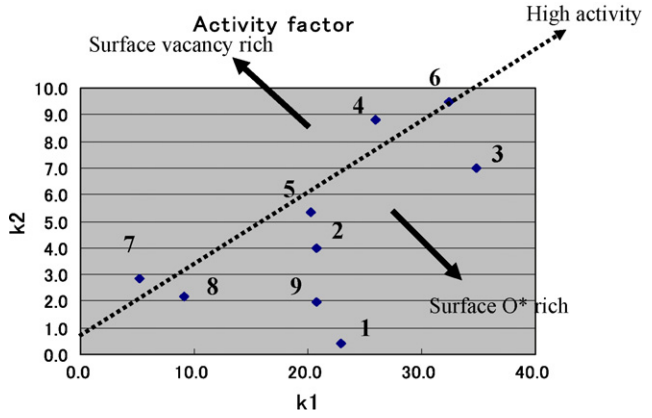

Fig. 8. Relation between k_1 and k_2 for the nine catalysts listed in Table 2.

catalysts are excellent. The transition metal-based catalysts (#7–9) exhibit low activity for methyl radical production. Under steady state conditions, the relative ratio of k_1 and k_2 (k_1/k_2) determines the surface concentration of active oxygen, as expressed in Eq. (6). Such a tendency can also be observed in Fig. 8. The $LiNO_3$/MgO (#1) catalyst surface is rich in active oxygen, but is not effective for the reaction with methane under these conditions.

In Fig. 9, $\log(k_4/k_3^2)$ is plotted as a function of x (Table 2). These parameters are related with the C2 selectivity. As shown in Fig. 2 (Eq. (3)) and Fig. 3 (Eq. (7)), $x/2$ is the order of O_2 pressure for the rate of methyl radical oxidation. Sinev et al. [18] have proposed that methyl radicals (under an equilibrium with methyl peroxide, Eq. (14)) can be oxidized in two ways (Eqs. (15) and (16)).

$$CH_3 + O_2 = CH_3O_2 \quad (14)$$

$$CH_3O_2 + CH_3O_2 \rightarrow CO \text{ and } CO_2 \quad (15)$$

$$CH_3O_2 + CH_3 \rightarrow CO \text{ and } CO_2 \quad (16)$$

From the proposed reactions, the CO_x production rate is a function of a 2nd order of methyl radical concentration and a 2nd (Eq. (15)) or 1st order (Eq. (16)) of oxygen pressure. Although the rate order for methyl radicals is different (2 by Sinev, 1 by Iwamatsu–Aika), the exponent of oxygen pressure ($x/2 = 2$ or 1; $x = 4$ or 2 in gas phase) is interesting. Another possibility is the oxidation of methyl peroxide through surface oxygen or gaseous oxygen, which implies the x to be in between 2 and 4. If the I–A model assumes that only surface oxygen is used for oxidation of methyl radicals (not methyl peroxide), $x/2$ can be lower than unity (x: below 2 for the surface reaction). Considering the above discussion, x can be estimated as a number between 0 and 4. In the present work, x between 1 and 4 was obtained (Table 2 and Fig. 9). The first result for the value of x was 1.6 for $NaNO_3$/MgO [17], and the second results were 0.7 or 1.0 for $NaNO_3/NiTiO_3$ [19].

Amorebieta and Colussi [6] stated that methyl radical is oxidized on the surface (oxygen) of SrO under low pressure (0.4 Pa). The rate is proportional to square root (or less than half order) of oxygen pressure, which means that x is lower than 1. We believe that the situation around the catalyst must be different because the pressure of our study (40,000 Pa) is quite different from them (0.4 Pa).

Although the rate constant for methyl radical recombination (k_4) may be established in the gas phase, the real reaction near the surface might be affected by the nature of the surface (such as the body effect, accepting the recombination energy). Methyl radical oxidation (k_3) is considered to occur with surface oxygen, in addition to gas phase oxygen, as previously discussed above. Thus, the factor that determines C2 selectivity, $\log(k_4/k_3^2)$, must depend on the nature of the catalyst. As shown in Fig. 9, $\log(k_4/k_3^2)$ is low for transition metal-based catalysts (#7–9), but high for $LiNO_3$/MgO (#1 and #6). The x value is also low for transition metal-based catalysts (#7–9). Therefore, it is proposed that methyl radical oxidation occurs more extensively with surface oxygen for the transition metal-based catalysts (#7–9). On the other hand, methyl radical oxidation might occur to a large extent in the gas phase for non-redox oxides such as $LiNO_3$/MgO (#1 and #6), which is also supported by a high value of x (Fig. 9).

5.2. Relationship between the kinetic parameters and the morphological nature of the catalysts

One of the present authors has demonstrated the role of morphology of the catalyst for OCM reaction [33,34]. Methyl radicals are produced at the surface, but combine in the gas phase to produce C2 compounds (heterogeneous–homogeneous reaction). The surface is necessary, but may destroy the methyl radicals through reaction with the surface oxides [33,34]. Su et al. [43] have pointed out the importance of micropore space for methyl radical recombination. It was proposed that there is a suitable morphology, or suitable specific surface area, that provides high C2 selectivity. For $NaNO_3$/MgO, it is a low surface area such as several m^2/g [33]. Most of the catalysts selected here exhibit such low surface areas ranging from 1 to 12 m^2/g (Fig. 10). For samples having such suitable surface areas, the discussion regarding the relationship with kinetic parameters may not be so important. However, such relationships are briefly discussed. Fig. 10

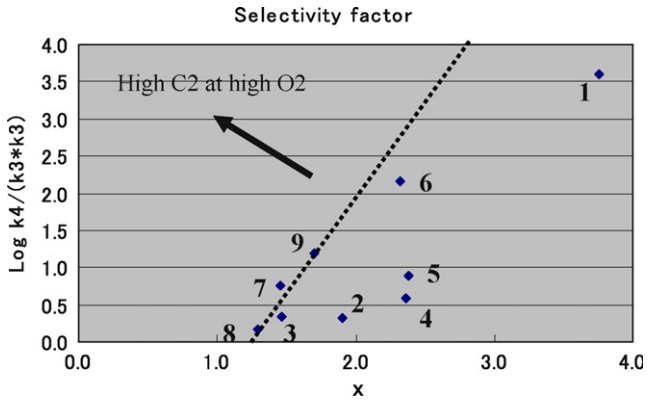

Fig. 9. Relation between $\log(k_4/k_3^2)$ and x for the nine catalysts listed in Table 2.

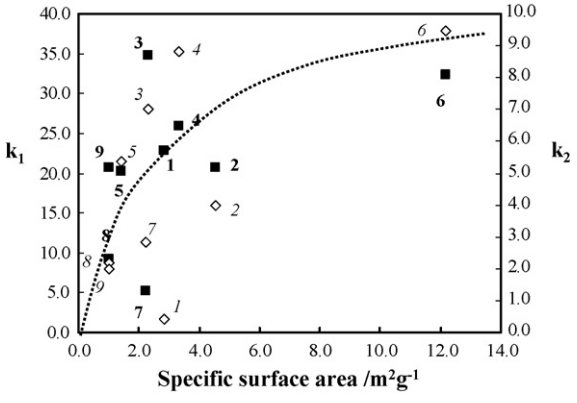

Fig. 10. Relation between the activity factors (closed symbol for k_1 and open symbol for k_2) and specific surface area for the nine catalysts listed in Table 2.

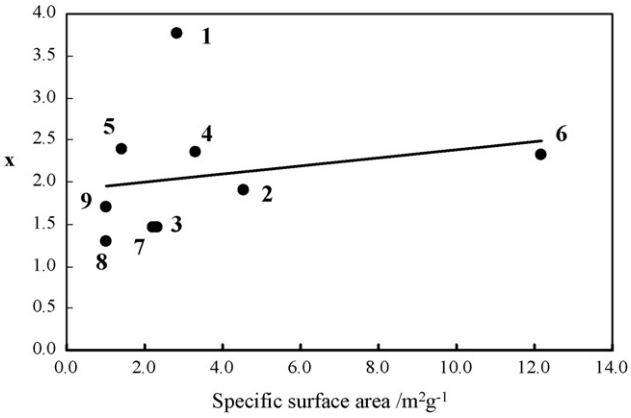

Fig. 11. Relation between the selectivity factor (x) and specific surface area for the nine catalysts listed in Table 2.

shows the relationship between the methyl radical production rate (k_1 and k_2) as a function of the specific surface area. Both k_1 and k_2 increase with the increase in the specific surface area. Methyl radical production is reasonably correlated with the surface area (if the chemical nature is almost the same). In Fig. 11, x is plotted as a function of the specific surface area, suggesting a poor or complicated relationship. The only comment to be made here is that $LiNO_3$/MgO (#1 and #6) has high x values, which may indicate that gas phase oxidation is more important than the surface oxidation for this sample or for this sample-installment.

5.3. Effect of reaction time or sulfate on the kinetic parameters

Fig. 12 shows the relation between k_1 and k_2 for the catalysts listed in Table 4, as reproduced in Fig. 8. The dotted arrows indicate the effect of reaction time; catalysts #1 to #(1), #5 to #(5), and #6 to #(6). Generally both k_1 and k_2 decreased with time, which indicates that the activity is decreased. The solid arrows show the effect of sulfate; catalysts #3 to #4, #5 to #11, and #6 to #12. Lithium sulfate decreases the activity (both k_1 and k_2), while sodium sulfate does not seem to significantly decrease activity.

Fig. 13 shows the relation between $\log(k_4/k_3^2)$ and x for the catalysts listed in Table 4, as reproduced in Fig. 9. The dotted arrows indicate the effect of reaction time; catalysts #1 to #(1), #5 to #(5), and #6 to #(6). Generally, both $\log(k_4/k_3^2)$ and x were decreased with time, which indicates that the C2 selectivity is decreased. The solid arrows show the effect of sulfate; catalysts #3

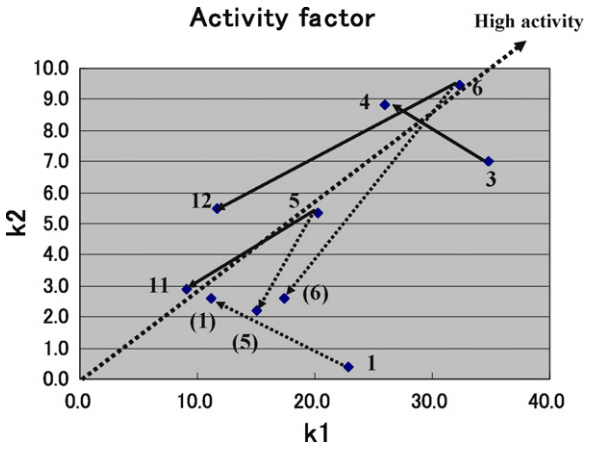

Fig. 12. Relation between k_1 and k_2 for the four groups of catalysts listed in Table 4.

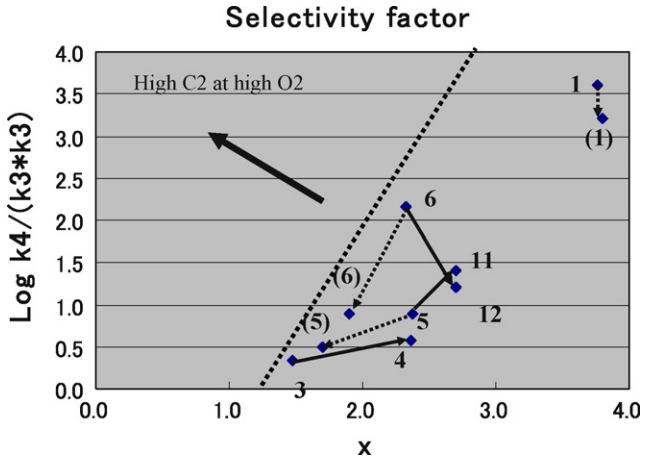

Fig. 13. Relation between $\log(k_4/k_3^2)$ and x for the four groups of catalysts listed in Table 4.

to #4, #5 to #11, and #6 to #12. $\log(k_4/k_3^2)$ is increased for catalysts #4 and #11, but is decreased for catalyst #12. The x value is increased for all cases. The effect of sulfate on the C2 selectivity seems to be complicated, while it might decrease at higher pressure, as discussed later.

5.4. Kinetic simulation under high pressure

The disadvantage of the I–A model is that secondary reactions such as C2 oxidation are ignored to maintain the simplicity of the model. Thus, the selectivity at high conversion cannot be calculated. On the other hand, the activity at low conversion can be estimated at any pressure. For industrial use, the C2 selectivity or C2 production rate at high pressure is necessary; however, most of the reported laboratory data are measured below atmospheric pressure. Therefore, catalysts that are effective under high pressure must be developed for industrial purposes.

The C2 selectivity of nine catalysts was calculated as a function of pressure (up to 200 kPa) and is shown in Fig. 14. The concentration ratio of methane/oxygen was fixed at four, the stoichiometry for ethene production. All the catalysts lose selectivity at high pressure, especially #1, #2, #4, and #5 show significant loss of selectivity. Based on the discussion of x, the gas phase reaction is more active for these catalysts. The parameters of those catalysts are located at high x and low $\log(k_4/k_3^2)$ in Fig. 9. The C2 selectivity is not significantly decreased

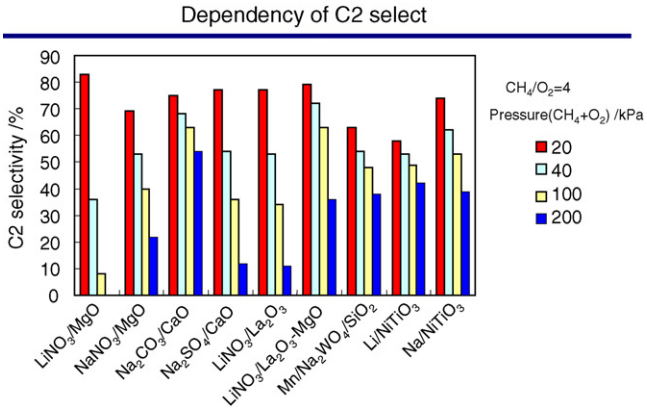

Fig. 14. C2 selectivity simulated using the I–A model for nine catalysts (Table 2) as a function of the reaction pressure. (For interpretation of the references to color in this artwork, the reader is referred to the web version of the article.)

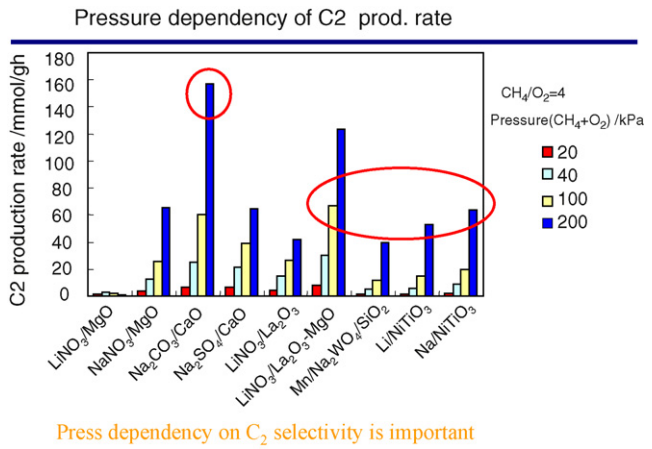

Fig. 15. C2 productivity simulated using the I–A model for nine catalysts (Table 2) as a function of the reaction pressure. (For interpretation of the references to color in this artwork, the reader is referred to the web version of the article.)

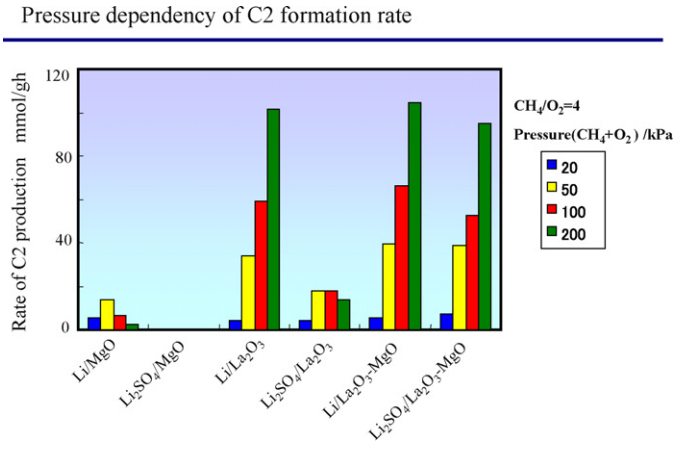

Fig. 17. C2 productivity simulated using the I–A model for six catalysts (Table 4) as a function of the reaction pressure. (For interpretation of the references to color in this artwork, the reader is referred to the web version of the article.)

for #3, #6–9, which could be suitable industrial catalysts. Those catalysts are located at low x and high $\log(k_4/k_3^2)$ in Fig. 9. It is interesting to note that the transition metal-based catalysts (#7–9) do not show significant loss of C2 selectivity under high pressure. These may be useful catalysts at higher pressures, as their parameters are located left and high in the graph of Fig. 9. It should be noted that for any of the catalysts under low pressure, the selectivity is generally high and similar (60–80%), so that the effectiveness of the catalyst cannot be determined under these conditions. However, at high pressure the difference is remarkable (10–50%), which demonstrates that the I–A model can give some guidelines to evaluate catalysts for practical use.

The C2 productivity of nine catalysts was calculated as a function of pressure (up to 200 kPa) and is shown in Fig. 15. The methane/oxygen concentration ratio is fixed at four, the stoichiometry for ethene production. The productivity of all the catalysts increases at high pressure up to 200 kPa, especially #3 and #6. The transition metal-based catalysts (#7–9) may show much higher C2 productivity under pressures higher than 200 kPa. The numerical number itself might not show the practical results if the experiments would be done, because the calculation is done under several restrictions. We would like to stress the importance of the trends.

The same calculation for C2 selectivity as a function of pressure was performed using the kinetic parameters taken after the 2-h runs (Table 4), and is shown in Fig. 16. Lithium-promoted catalysts exhibit a significant loss in selectivity at high pressure (compare #5 and #6 of Fig. 14 and #(5) and #(6) of Fig. 16). Sulfate-promoted catalysts (#11 and #12 vs. #5 and #6) do not exhibit high selectivity at high pressure. The values for the $\log(k_4/k_3^2)$ parameter were changed to lower values, but x was moved to higher values (Fig. 13). This suggests that the reaction occurs more in the gas phase, which may be a reason for the poor selectivity. The same calculation for C2 productivity as a function of pressure was also performed using the kinetic parameters taken after the 2-h runs (Table 4), and is shown in Fig. 17. Lithium-promoted catalysts did not exhibit significantly high productivity at high pressure (compare #5 and #6 of Fig. 15 and #(5) and #(6) of Fig. 17). The sulfate-promoted catalysts (#11 and #12 vs. #5 and #6) also did not exhibit significantly high productivity at high pressure. The sulfate-promoted catalysts had values for C2 productivity similar to the nitrate-promoted catalysts for the 2-h runs at high pressure (Fig. 17).

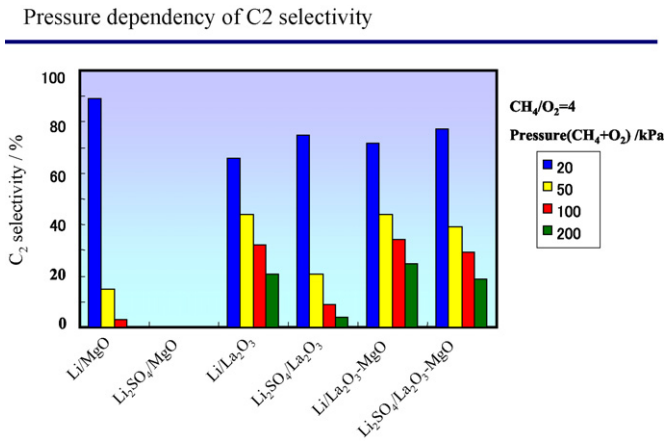

Fig. 16. C2 selectivity simulated using the I–A model for six catalysts (Table 4) as a function of the reaction pressure. (For interpretation of the references to color in this artwork, the reader is referred to the web version of the article.)

6. Conclusions

Much of the research regarding OCM kinetics that has been reported was classified into six categories and evaluated. From the standpoint of catalyst design, the model developed by Iwamatsu and Aika was selected and used for a kinetic analysis of the OCM reaction. The model can supply four parameters, two of which (k_1 and k_2) are related to activity and two ($\log(k_4/k_3^2)$ and x) of which are related to selectivity. Twelve alkali metal-promoted catalysts, which have been reported as effective for the OCM reaction, were prepared and used for the kinetic study. The I–A model was confirmed to be successfully applicable and the parameters were discussed in relation with the chemical or physical nature of the catalysts.

Na_2CO_3/CaO and $LiNO_3/La_2O_3$–MgO catalysts have high activity (high k_1 and k_2) and moderate selectivity (high $\log(k_4/k_3^2)$ and low x). These catalysts are considered to have high densities of active surface oxygen, and exhibit controlled gas phase oxidation reaction (low x). The C2 selectivity and productivity of these catalysts under pressures up to 200 kPa were calculated using the I–A model, and both were confirmed to be high.

The $MnO/Na_2WO_4/SiO_2$, $LiOH/NiTiO_3$, and $Na_2CO_3/NiTiO_3$ transition metal-based catalysts have rather low activity (low k_1 and k_2), but high selectivity (high $\log(k_4/k_3^2)$ and low x). The low activity is related with their low surface area (1–2 m^2/g). The C2 selectivity and productivity of these catalysts under a pressure of

200 kPa were calculated using the I–A model, and was confirmed to be high and medium. If a technique to increase the specific surface area of these catalysts is developed, then they would be good candidates for industrial use.

Lithium nitrate-promoted catalysts gradually lose their activity; however, the surface lithium contents were not drastically changed (as determined by XPS). Over the reaction time, the kinetic parameters gradually change, and this is considered to be due to the change in the nature of the active site over time. Alkali metal sulfates were used instead of nitrates to improve the catalyst stability; however, the selectivity or the kinetic parameters were not improved.

The potential of the I–A model for the evaluation of OCM catalysts was demonstrated for the future prospects of OCM technology, although the exact yield and selectivity for each catalyst under the practical condition cannot be given with this model.

References

[1] K. Aika, J.H. Lunsford, J. Phys. Chem. 81 (1977) 1393.
[2] (a) D.J. Driscoll, W. Martin, J.H. Ji-Xiang Wang, Lunsford, J. Am. Chem. Soc. 107 (1985) 58;
(b) T. Ito, J.H. Lunsford, J. Am. Chem. Soc. 107 (1985) 5062.
[3] K.D. Campbell, J.H. Lunsford, J. Phys. Chem. 92 (1988) 5292.
[4] Y. Tong, M.P. Rosynek, H. Lunsford, J. Phys. Chem. 93 (1989) 2896.
[5] Y. Feng, J. Niiranen, D. Gutman, J. Phys. Chem. 95 (1991) 6558.
[6] V.T. Amorebieta, A.J. Colussi, J. Am. Chem. Soc. 117 (1995) 3856.
[7] K.J. Laidler, Chemical Kinetics 1950, 2nd ed., McGraw-Hill, Inc, 1965.
[8] I.R. Slagle, D. Gutman, J. Am. Chem. Soc. 107 (1985) 5342.
[9] H. Zanthoff, M. Baerns, Ind. Eng. Chem. Res. 29 (1990) 2.
[10] J.W.M.H. Geerts, Q. Chen, J.M.N. van Kasteren, K. van der Wiele, Catal. Today 6 (1990) 519.
[11] Y. Zin, Z. Song, Y.Z. Tan, D. Wang, Catal. Today 131 (2008) 483.
[12] J.A. Labinger, K.C. Ott, J. Phys. Chem. 91 (1987) 2682.
[13] P.F. Nelson, N.W. Cant, J. Phys. Chem. 94 (1990) 3756.
[14] J.H. Kolts, J.B. Kimble, R. Porter, ACS Meeting, 1991.
[15] K. Asami, T. Shikada, K. Fujimoto, H. Tominaga, Ind. Eng. Chem. Res. 26 (1987) 2348.
[16] Yu.I. Pyatnitsky, N.I. Ilchenko, M.V. Pavlenko, Catal. Today 42 (1998) 233.
[17] E. Iwamatsu, K. Aika, J. Catal. 117 (1989) 416.
[18] M.Yu. Sinev, V.N. Korchak, O.V. Krylov, Kint. Katal. 28 (1987) 1376, 30 (1989) 855.
[19] E.E. Miro, J.M. Santamaria, E.E. Wolf, J. Catal. 124 (1990) 465.
[20] L. Lehman, M. Baerns, J. Catal. 135 (1992) 467.
[21] S.K. Agarwal, R.A. Migone, G. Marcelin, J. Catal. 123 (1990) 228.
[22] D. Wolf, R. Moros, Chem. Eng. Sci. 52 (1997) 1189.
[23] D. Wolf, M. Slinko, E. Kurkina, M. Baerns, Appl. Catal. A 166 (1998) 47.
[24] D. Wolf, M. Heber, W. Grunert, M. Muhler, J. Catal. 199 (2001) 92.
[25] K. Otsuka, K. Jinno, Inorg. Chem. Acta 121 (1986) 237.
[26] V.T. Amorebieta, A.J. Colussi, J. Phys. Chem. 92 (1988) 4576.
[27] A.J. Roos, S.J. Korf, R.H.J. Veehof, J.G. van Ommen, J.R.H. Ross, Appl. Catal. 52 (1989) 131.
[28] A.M. Efstathiou, D. Boudouvas, N. Vamvouka, X.E. Verykios, J. Catal. 140 (1993) 1.
[29] I.T. Ali Emesh, Y. Amenomiya, J. Phys. Chem. 90 (1986) 4785.
[30] J.M. Santamaria, E.E. Miro, E.E. Wolf, Ind. Eng. Chem. Res. 30 (1991) 1157.
[31] S.M. Al-Zahrani, Catal. Today 64 (2001) 217.
[32] N. Yaghobi, M.H.R. Ghoreishy, J. Nat. Gas Chem. 17 (2008) 8.
[33] E. Iwamatsu, T. Moriyama, N. Takasaki, K. Aika, J. Catal. 113 (1988) 25.
[34] T. Nishiyama, T. Watanabe, K. Aika, Catal. Today 6 (1990) 391.
[35] X. Fang, S. Li, J. Lin, J. Gu, D. Yan, J. Mol. Catal. (China) 6 (1992) 427.
[36] M.P. Carlier, A.B. Hadid, C.J. Cameron, J. Stud. Surf. Sci. Catal. 61 (1991) 183.
[37] Y. Osada, S. Koike, T. Fukushima, S. Ogasawara, Appl. Catal. 59 (1990) 59.
[38] R. Spinicci, P. Marini, S.De. Rossi, M. Faticanti, P. Porta, J. Mol. Catal. A: Chem. 176 (2001) 253.
[39] V.R. Choudhary, V.H. Rane, S.T. Chaudhari, Appl. Catal. 158 (1997) 121.
[40] V.R. Choudhary, V.H. Rane, S.T. Chaudhari, Fuel 79 (2000) 1487.
[41] H. Aritani, H. Yamada, T. Nishio, T. Shiono, S. Imamura, M. Kudo, S. Hasegawa, T. Tanaka, S. Yoshida, J. Phys. Chem. B 104 (2000) 10133.
[42] I. Cambell, S. Saricilar, I.C. Hoare, S.K. Bhargava, Appl. Catal. 82 (1992) 13.
[43] Y.S. Su, J.Y. Ying, W.H. Green Jr., J. Catal. 218 (2003) 321.